Using microearthquakes to track repeated magma intrusions beneath the Eyjafjallajökull stratovolcano, Iceland

Jon Tarasewicz,[1] Bryndís Brandsdóttir,[2] Robert S. White,[1] Martin Hensch,[2] and Bergthóra Thorbjarnardóttir[3]

Received 7 August 2011; revised 25 November 2011; accepted 29 November 2011; published 7 February 2012.

[1] We have mapped microearthquakes caused by magma migration preceding and during the flank and summit eruptions in March–May 2010 of Eyjafjallajökull stratovolcano in Iceland using a Coalescence Microseismic Mapping technique. Spatial and temporal clustering of >5,000 microearthquakes under the eastern flank of the volcano illuminates several northeast–southwest striking sub-vertical dikes at 2–6 km b.s.l., emplaced before the Fimmvörðuháls flank eruption in March. This intense precursory seismicity had a lateral extent of ∼6 km east-west and ∼3 km north-south. A sequence of 386 microearthquakes during the summit eruption, refined by double-difference relative relocation, defines a sub-linear trend inclined ∼5–10° from vertical extending from the upper mantle at ∼30 km depth to the summit crater. This sequence includes two major clusters at ∼19 km and ∼24 km b.s.l., each containing >100 earthquakes. All microearthquakes display characteristics of brittle fracture, with several subsets of events exhibiting closely similar waveforms within clusters. This suggests similar, repetitive source processes. The deeper clusters may be caused by fracturing solidified magma plugs that form constrictions in an otherwise aseismic melt conduit. Or they may occur at exit points from melt pockets, in which case they indicate positions of magma storage at depth. The seismicity deeper than 10 km only starts three weeks after the onset of the summit eruption, after which the largest clusters occur at progressively greater depths. This temporal pattern may result from pressure release at shallow levels in the magmatic plumbing system progressively feeding down to mobilize deeper melt pockets.

Citation: Tarasewicz, J., B. Brandsdóttir, R. S. White, M. Hensch, and B. Thorbjarnardóttir (2012), Using microearthquakes to track repeated magma intrusions beneath the Eyjafjallajökull stratovolcano, Iceland, *J. Geophys. Res.*, *117*, B00C06, doi:10.1029/2011JB008751.

1. Introduction

[2] The ice-capped Eyjafjallajökull stratovolcano is located in the propagating southern part of the Eastern Volcanic Zone (EVZ) in South Iceland (Figure 1). Northwest of Eyjafjallajökull, the EVZ intersects with the South Iceland Seismic Zone (SISZ), which accommodates overall left-lateral motion along an east-west transform by bookshelf faulting on right-lateral north-south oriented strike-slip faults [*Einarsson*, 1991]. South of the intersection with the SISZ, the EVZ is characterized by large volcanoes and a lack of conspicuous rift structures. The east-west elongated Eyjafjallajökull stratovolcano is linked to the larger adjacent Katla volcanic system through east-west striking faults and eruptive fissures (Figure 1).

[3] Although tectonically connected, the eruption histories of these two volcanoes are markedly different. The subglacial Katla system is one of the most active volcanoes in the EVZ with more than twenty documented historic eruptions [*Larsen*, 2000] and persistent seismic activity [*Einarsson and Brandsdóttir*, 2000; *Jakobsdóttir*, 2008]. In contrast, Eyjafjallajökull has only two known historical eruptions, in 1612 and 1821–1823 [*Thoroddsen*, 1925; *Larsen*, 1999], and prior to 1991 was seismically quiet. Soil profiles indicate that the 4.5 km long, NW ridge of Eyjafjallajökull (Skerin) formed synchronously with an eruption in Katla in 920 A.D [*Óskarsson*, 2009]. These eruptions were followed by the ∼75 km long 934 A.D. Eldgjá fissure eruption, formed by rifting to the northeast of the Katla caldera (Figure 1).

[4] Intense seismic swarms beneath Eyjafjallajökull in 1994, 1996 and 1999–2000 delineated pathways of recent magma intrusions into the volcano [*Hjaltadóttir et al.*, 2009]. In 1994 and 1999 magmatic intrusions are inferred to have been emplaced at a depth of 3.5–6.5 km beneath the volcano based on surface deformation measurements and seismicity [*Sturkell et al.*, 2003; *Pedersen and Sigmundsson*, 2004, 2006; *Dahm and Brandsdóttir*, 1997]. Seismicity associated with the 1996 intrusion was predominantly at much greater

[1]Bullard Laboratories, University of Cambridge, Cambridge, UK.
[2]Institute of Earth Sciences, Science Institute, University of Iceland, Reykjavík, Iceland.
[3]Icelandic Meteorological Office, Reykjavík, Iceland.

0148-0227/12/2011JB008751

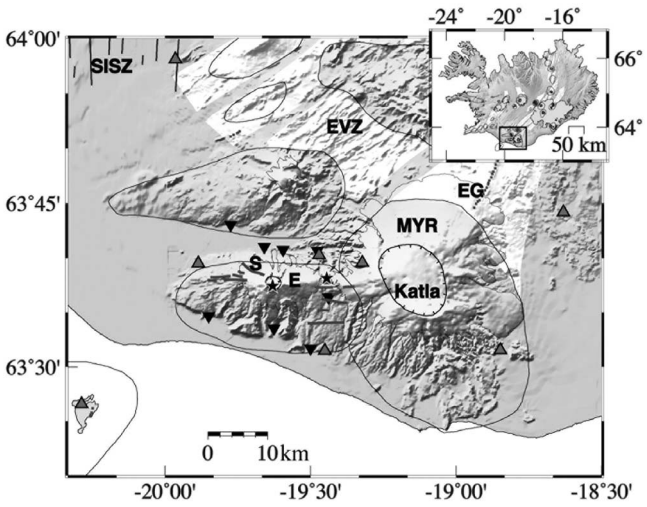

Figure 1. A tectonic map of the subglacial Eyjafjallajökull (E) and Katla volcanoes. Inset shows tectonic map of Iceland, with data adapted from *Einarsson and Sæmundsson* [1987]. Thin black lines show the extent of glaciers, which are shaded gray in inset. Thicker black lines indicate outlines of central volcanoes. Their associated fissure swarms are shown in white. Tick-marked lines show outlines of summit craters and calderas. Dark gray lines indicate Holocene faults and eruption fissures. Black stars show the flank and summit eruption sites. East–West aligned faults and fissures characterize Eyjafjallajökull [*Jóhannesson and Sæmundsson*, 1998; P. Einarsson and A. R. Hjartardóttir, Structure and tectonic position of the Eyjafjallajökull volcano, southern Iceland, manuscript in preparation, 2012]. The NW Skerin ridge (S) formed synchronously with the 934 A.D. Eldgjá (EG) eruption northeast of the Katla caldera. Temporary seismometers deployed by the University of Iceland are denoted by inverted triangles and stations within the permanent IMO-operated network are shown by upright gray triangles.

depths of 20–25 km, indicating the emplacement of an intrusion at the base of the crust [*Hjaltadóttir et al.*, 2009].

[5] Bimodal petrology of postglacial eruption fissures that radiate away from the 2.5 km wide summit crater of Eyjafjallajökull indicate that they were sourced from crustal magma chambers containing both mafic and silicic components [*Jóhannesson and Sæmundsson*, 1998; *Óskarsson*, 2009]. A shallow (1.5 km below sea level) magma chamber has been inferred beneath Katla from seismic undershooting data [*Gudmundsson et al.*, 1994]. However, no equivalent seismic refraction data exist for Eyjafjallajökull.

[6] On 20 March 2010, a basaltic fissure eruption began at Fimmvörðuháls on the eastern flank of Eyjafjallajökull and continued until 12 April 2010 (Figure 2). On 14 April, a second, explosive eruption began at the ice-covered summit of the volcano, 8 km west of the first eruption site. This second eruption continued with variable intensity until mid-June 2010 and was characterized by a more silicic (trachyandesite) magma than the basaltic fissure eruption and by a fine-grained ash plume that rose to heights of 6–9 km [*Sigmundsson et al.*, 2010]. The height of the initial plume was partly controlled by magma-ice interaction generating explosive activity. The eruptions were preceded by a period of geodetically inferred inflation and escalating seismicity beneath the volcano in December 2009 to March 2010, with the most rapid deformation and most active seismicity occurring in March 2010 [*Sigmundsson et al.*, 2010]. This paper discusses the seismicity recorded during this highly

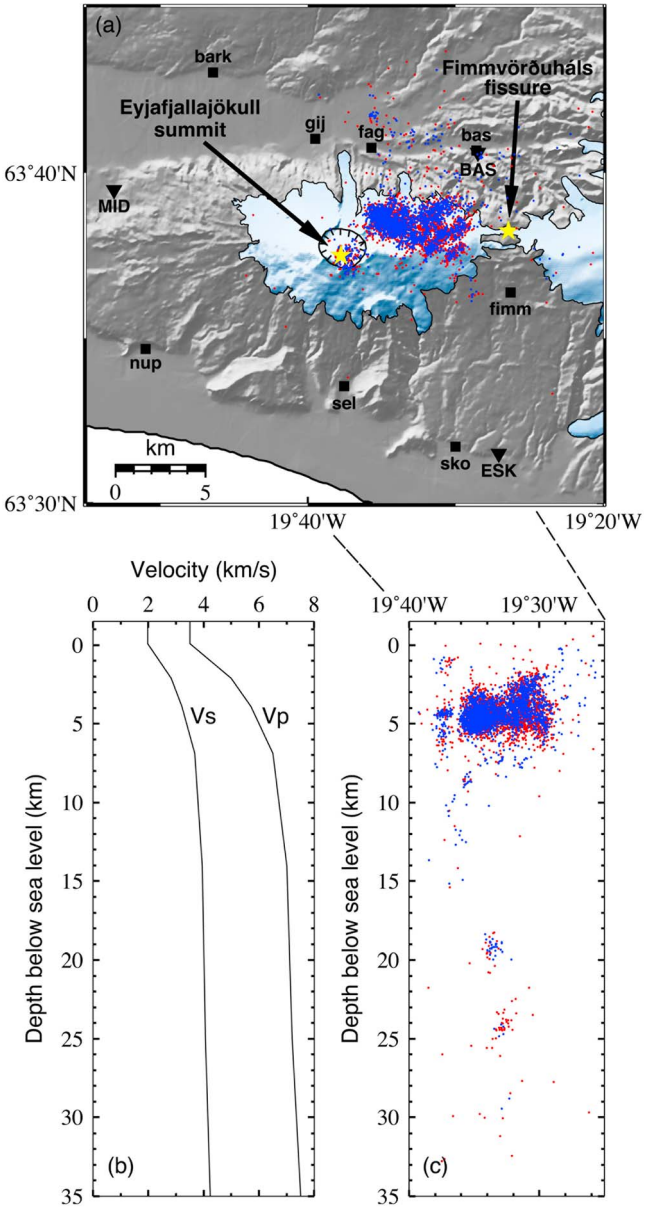

Figure 2. (a) Overview map showing CMM epicenter locations detected during the entire twelve-week period from 6 March to 31 May 2010. Red dots are earthquakes with SNR > 2.5; blue dots are earthquakes with SNR > 2.75. The Fimmvörðuháls and Eyjafjallajökull summit eruption sites are marked by yellow stars. Seismometer locations are marked by black squares (University of Iceland temporary deployment, labeled in lower case) and inverted black triangles (IMO permanent network, labeled in upper case). (b) The 1-D velocity model used to locate earthquake hypocenters (see Table 1 for details). (c) E-W cross-section of the same seismic events shown in Figure 2a.

Table 1. Seismometer Station Locations[a]

Station Name	Latitude (deg)	Longitude (deg)	Elevation (m)
fimm	63.6066	−19.4376	861
bark	63.7170	−19.7753	129
sko	63.5286	−19.4998	49
nup	63.5779	−19.8504	33
sel	63.5590	−19.6258	74
fag	63.6795	−19.5949	194
bas	63.6780	−19.4767	255
gij	63.6839	−19.6587	166
BAS	63.6770	−19.4744	240
ESK	63.5250	−19.4508	95
GOD	63.6598	−19.3224	1200
HAU	63.9685	−19.9647	96
HVO	63.5261	−18.8478	196
MID	63.6583	−19.8857	132
SNB	63.7364	−18.6307	245
VAT	63.1866	−18.9177	573
VES	63.4429	−20.2866	55

[a]Lower-case station names are temporary deployments by the University of Iceland; upper-case station names are permanent stations operated by the Icelandic Meteorological Office. Geoid used is WGS84.

active period immediately preceding the eruptions, through the main period of activity of both eruptions.

2. Data Acquisition

[7] Six Reftek RT130–01 three-component seismometers using Lennartz 5s sensors were deployed at temporary stations on 5 March 2010 around Eyjafjallajökull, sixteen days before the Fimmvörðuháls eruption began on 20 March. In addition to these, we have used data from nine stations in the permanent seismometer network operated by the Icelandic Meteorological Office (IMO), which cover the wider area around Eyjafjallajökull and Fimmvörðuháls (Figure 1 and Table 1). The data used in this study cover the period from 5 March 2010 until the end of May 2010, encompassing the entire duration of the Fimmvörðuháls fissure eruption (20 March to 12 April) and the first six weeks of the Eyjafjallajökull summit eruption (14 April to mid-June). All data were recorded at a sampling rate of 100 samples per second with a GPS time base.

3. Hypocenter Location

3.1. Velocity Model

[8] Hypocenter locations were obtained using a transversely isotropic 1-D velocity model with linear velocity gradients (Figure 2 and Table 2), based on the southeastern end of the SIST refraction profile [*Bjarnason et al.*, 1993] and the northern part of the Katla refraction profile [*Gudmundsson et al.*, 1994]. Both profiles have similar velocity gradients and upper crustal thickness. We use a constant V_p/V_s ratio of 1.77, based on values derived from Wadati plots [*Wadati*, 1933] of manually picked event arrival times (Figure S1 of the auxiliary material).[1] We did not insert a velocity step at the Moho, partly because its depth is not well known and partly because such steps tend to cause hypocenters to cluster in their vicinity. However, the best estimate of Moho depth here is 22–23 km based on a combination of wide-angle reflection and refraction profiling and gravity modeling [*Darbyshire et al.*, 2000; *Brandsdóttir and Menke*, 2008; *Vogfjörð et al.*, 2002].

3.2. Coalescence Microseismic Mapping

[9] We use the Coalescence Microseismic Mapping (CMM) technique [*Drew*, 2010; *Brandsdóttir et al.*, 2010] to automatically detect and locate seismic events in our data set. The method has a theoretical basis in the Bayesian inversion of arrival times [*Tarantola and Valette*, 1982], with the purpose of imaging for the detection and location of an event without reducing the data to discrete arrival time picks. Given a defined search volume of the subsurface and a velocity model, the CMM program migrates seismic energy from each receiver back into the subsurface searching for times and locations where the energy focuses. The resultant spatiotemporal maps identify likely times and locations of seismic events, as points of coalescence of the migrated signals.

[10] Before running a search on the data, the CMM program forward-models P- and S-wave travel times from each node of the search grid to each receiver in the network. This produces a comprehensive travel time 'look-up table' that is then used for the migration. The program then performs a continuous search of the seismic data by computing an 'onset' function based on a short-term average versus long-term average (STA/LTA) algorithm, which is calculated for both the vertical and the combined horizontal components at each station. A maximum in the STA/LTA onset function at a station corresponds to a possible arrival, although the identification of a discrete arrival is not required by the method. A 'coalescence' function is computed at each node of the grid by migrating the STA/LTA onset functions from each station using the look-up table of forward-modeled travel times to create a spatial coalescence map, which evolves with time. The weighting of each station within the coalescence function is directly dependent on the magnitude of the onset function at each station, hence station weighting objectively varies with the observed signal-to-noise ratio of the data. The coalescence function reaches a maximum at the grid node and event origin time that best match both the P-wave and the S-wave detected arrivals at all the stations. A detection threshold is chosen to return location estimates for as many real events as possible without producing an unacceptable number of false triggers.

[11] To reduce errors in the location estimate arising from travel time residuals caused by deviations from the 1-D velocity model, the CMM program integrates the coalescence function over a time window chosen to encompass the maximum estimated travel time residual. The resultant spatial map is then smoothed and a Gaussian function is fitted at

Table 2. Velocity Model Parameters Used to Obtain Earthquake Hypocenter Locations

Depth Below Sea Level (km)	V_p (km s^{-1})	V_s (km s^{-1})
−1.5	3.50	1.98
0	3.50	1.98
2.2	5.00	2.83
4.0	5.70	3.22
7.0	6.50	3.67
14.0	7.00	3.96
25.0	7.20	4.07
35.0	7.50	4.24
40.0	7.60	4.29

[1]Auxiliary materials are available in the HTML. doi:10.1029/2011JB008751.

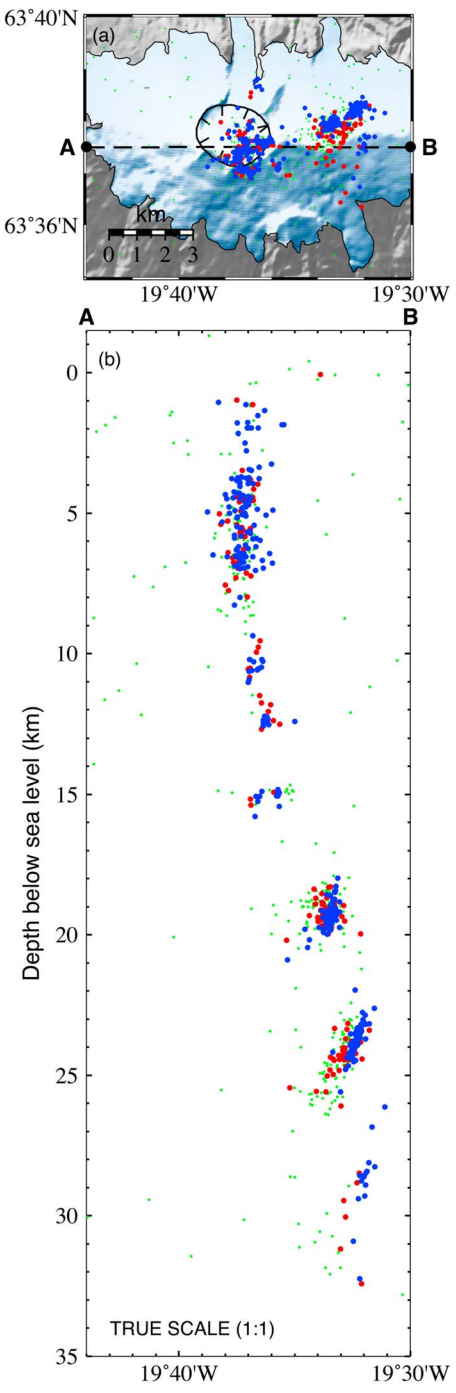

Figure 3. Comparison of CMM hypocenters with manually refined and relocated hypocenters. (a) map and (b) east-west cross-section along line A-B, showing hypocenters of earthquakes during the period 3–17 May 2010. Blue dots (386 events) show earthquakes that have been located with Hypoinverse and relocated with HypoDD, based on manual P- and S-wave arrival time picks. Red dots (137 events) show CMM locations with a SNR > 2.5, that is, those with a stronger coalescence value in the location algorithm. Small green dots (318 events) show CMM locations with 2.0 < SNR < 2.5, namely those with lower coalescence values. See text for discussion.

its local maximum, returning a time-averaged, best fit event location with the highest posterior probability. This 'mean' location is no longer tied to a grid node.

[12] The location technique employed by the CMM software removes the need to reduce the data to discrete arrival time picks or to apply subjective weighting to arrival picks. By virtue of continuously mapping the STA/LTA algorithm of the signal, noisy arrivals with low signal-to-noise ratio are automatically reduced in weight in the coalescence function in an objective fashion. While an STA/LTA maximum at an individual station may not always reflect a 'genuine' phase arrival, a false trigger (one which is unrelated to a seismic event inside the search volume) in the coalescence function can only occur if the local maximum at that station correlates with sufficiently high STA/LTA values at other stations, at the appropriate times, to generate a trigger above the detection threshold for the whole network. This is unlikely for a noise source close to an individual station and hence the method is robust against spurious, uncorrelated, local STA/LTA peaks.

[13] Furthermore, for instances when it is not obvious which is the real phase arrival by visual inspection of the seismic data, the signal information from the real arrival is still included in the CMM mean location, provided that the time window chosen for integration of the coalescence function encompasses it. By contrast, making an incorrect discrete arrival time pick and assigning a subjective weight to it, as is typical of other location methods, guarantees that the real arrival makes no contribution to the location solution and that location errors are actively introduced by the mis-pick.

[14] Although the identification of an arrival time is not necessary for the CMM location method, the program outputs estimated arrival times based on the local STA/LTA maximum at each station for each event that is identified. These automatically picked arrival times can be used to estimate travel time residuals compared to the forward-modeled travel times to each station from the event location. They can also be used to ascertain which STA/LTA maxima the program has detected and interpreted as an event, allowing rejection of events that are obviously false triggers.

[15] An initial catalog of 24,000 detected 'events' was generated by a CMM search over the whole twelve-week data set using a grid spacing of 400 m and a detection threshold of 2.0 signal-to-noise ratio (SNR) in a search volume 25 × 25 × 36.5 km (E-W × N-S × depth) centered at 63.63°N, 19.52°W. The seismic data were band pass filtered at 6–25 Hz for this stage. This full catalog of CMM events is likely to include some false triggers, but could easily be filtered by SNR value and location error estimates to give a smaller catalog of events that have a higher probability of being genuine earthquakes that are well located.

3.3. Relative Hypocenter Relocations

[16] The automatic CMM hypocenter locations reveal that much of the earthquake activity was concentrated in spatially separated clusters. To constrain individual clusters and to test CMM locations, we visually identified and manually picked P- and S-wave arrival times for a subset of 590 earthquakes. 204 of these occurred prior to the flank eruption in March 2010; 386 occurred in May 2010 during the summit eruption. Those time picks were used to derive single-event locations with Hypoinverse [*Klein*, 2002] and relative event

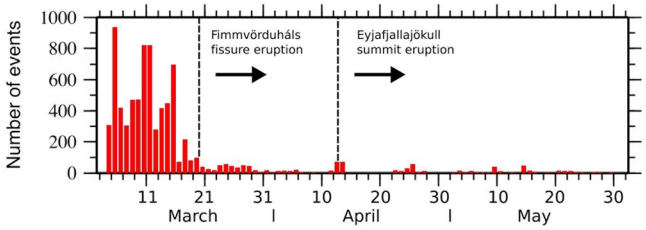

Figure 4. Histogram showing number of events recorded per day with a CMM signal-to-noise ratio (SNR) of >2.4 from 5 March to 31 May 2010. Note that most seismic activity occurred prior to the Fimmvörðuháls fissure eruption, with later bursts at the onset of the Eyjafjallajökull summit eruption and in mid-May.

relocations with HypoDD, which employs a double-difference relocation algorithm [*Waldhauser and Ellsworth*, 2000].

[17] The relocation procedure also serves to validate our CMM hypocenters by comparison with well-established location algorithms. Locations from a data set of 318 CMM events with SNR between 2.0 and 2.5 (green dots in Figure 3) and 137 CMM events with SNR > 2.5 (red dots in Figure 3) that all occurred during the summit eruption, are compared with 386 of the same events after manual refinement and relocation of hypocenters (blue dots in Figure 3). CMM locations with lower SNR (green dots) tend to exhibit greater scatter compared to the relocated hypocenters, and 68 of these events were rejected as poorly constrained during the manual picking and relocation process. However, CMM hypocenters with higher coalescence (SNR > 2.5, red dots) closely match the distribution pattern of the relocated hypocenters (blue dots), and only one of these events was rejected during manual refinement and relocation. The close match between the CMM hypocenters with higher SNR values and the manually refined relocations suggests that the broad patterns of seismicity shown in Figure 2 are well represented by CMM hypocenters filtered by higher SNR values.

[18] Differences between CMM and Hypoinverse or HypoDD hypocenter locations are most likely driven by differences in station weightings and the treatment of station elevations. Station weightings in CMM are objectively based on the SNR observed at each station, in contrast to the subjective pick weightings applied in Hypoinverse and HypoDD. Station elevations in CMM are fully accounted for in the forward-modeled travel times calculated from each node in the search grid. This is not the case for Hypoinverse, which assumes a flat reference datum with station elevations accounted for by applying static time corrections. We have set the Hypoinverse reference level at sea level and applied static corrections calculated from the travel time at the surface velocity for a vertical raypath from sea level to the station. The static correction in particular can have considerable influence on the depth of hypocenter solutions. All earthquake depths discussed in this paper are relative to sea level, unless stated otherwise.

4. Location Results

[19] A temporal overview of seismicity observed during the twelve-week study period (Figure 4) illustrates the abrupt decrease in activity at the initiation of the Fimmvörðuháls eruption and a slight increase at the onset of the Eyjafjallajökull eruption. The local moment magnitudes (M_L) of the earthquakes that were recorded during this period by the Icelandic Meteorological Office (IMO) permanent network are small, with only three events larger than 3 and 98% of events during 5 March to 31 May having M_L below 2.

4.1. Seismicity Preceding and During the Fimmvörðuháls Fissure Eruption (20 March to 12 April 2010)

[20] The majority of the pre-eruptive seismicity was concentrated at depths of 3–6 km below sea level under the northeastern flank of Eyjafjallajökull, between the two eruption sites (Figures 2 and 5). During 5–20 March, the seismic activity migrated eastward toward the Fimmvörðuháls eruption site, forming a complex pattern of spatially and temporally separate seismic clusters (Figure 5).

[21] We have refined arrival time picks manually and obtained relative hypocenter relocations for 204 earthquakes on 14 March within the cluster furthest to the southeast (Figures 5 and 6 and Animation 1).[2] This cluster formed during 13–15 March, with 14 March being the most active. The automatic locations obtained with CMM, which delineate a distinct vertically elongated NE-SW aligned cluster, are resolved further by manual picking and relative relocation into three much tighter, sub-linear, vertically elongated clusters with a vertical extent of ~2 km. We interpret this seismicity as being associated with individual dikes. Manual picking and location using Hypoinverse of events from a separate cluster on 16 March also confirms the pattern of CMM locations and the northeast-southwest elongation of that cluster (H. Gunnarson, personal communication, 2011).

[22] During the Fimmvörðuháls fissure eruption, seismic activity continued at a relatively subdued level in the same region as the pre-eruption seismicity, primarily at the northeastern edge of the epicentral area shown in Figure 5.

4.2. Deep (>10 km) Seismicity During the Explosive Eyjafjallajökull Summit Eruption (14 April to Mid-June 2010)

[23] Seismic activity increased again only hours before the Eyjafjallajökull summit eruption began on 14 April (Figure 4). The seismicity accompanying the early stages of the summit eruption was concentrated in a sub-vertical 'pipe' directly beneath the eruption site extending down to ~5 km below sea level, with most events located in two distinct depth bands at 1–2 km b.s.l. and 4–5 km b.s.l. (Figure 7). The deeper of these is in agreement with the geodetic modeling of *Sigmundsson et al.* [2010], who suggest a deflating source beneath the summit crater at a depth of 4.0–4.7 km (relative to an average reference surface at ~400–500m a.s.l.) to explain the observed surface deformation during the early stages of the summit eruption. The seismicity suggests that there may also have been a second, shallower magma source at ~1–2 km depth b.s.l.

[24] Subsequent to the relatively shallow seismicity associated with the onset and early stages of the summit eruption was a period with much deeper seismicity. Figure 7 shows hypocenter locations during the period 13 April to 17 May,

[2] Animations are available in the HTML.

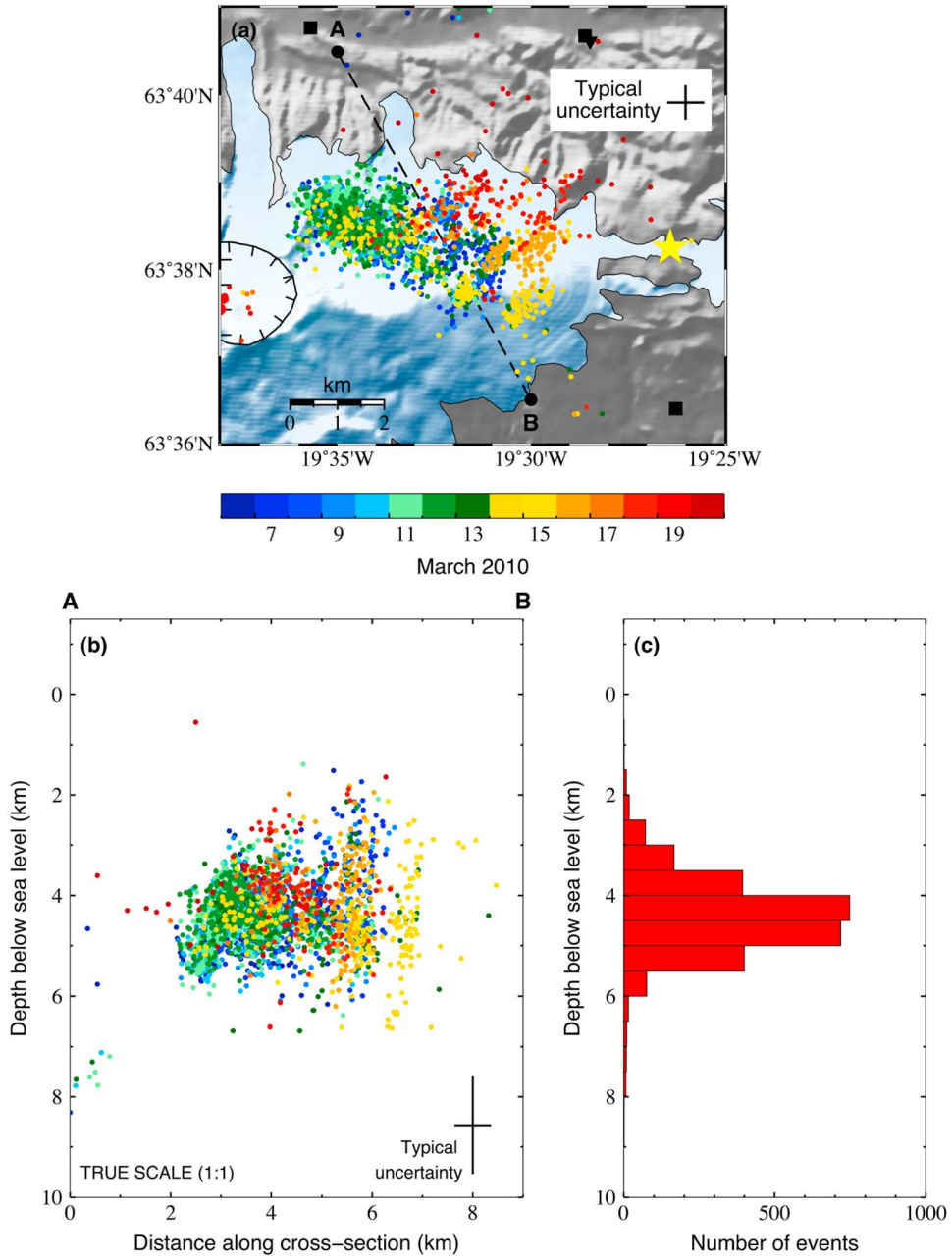

Figure 5. (a) CMM epicenter locations during 6–20 March 2010. Only CMM events with SNR > 2.5, horizontal uncertainty <1 km and vertical uncertainty <2.5 km are plotted, totaling 2,647 events. The glacier is shaded in light blue. Circles are earthquake epicenters color-coded by date. Yellow star shows location of the Fimmvörðuháls fissure eruption on 20 March 2010, black squares are temporary seismometer sites, black inverted triangles are permanent seismometer sites. (b) Cross-section showing the same events projected onto dashed line A–B shown in Figure 5a. Typical uncertainty shown is the mean value of all events plotted. (c) Histogram of depth distribution for events plotted in Figures 5a and 5b showing that most activity was located between 3 and 6 km below sea level.

obtained using CMM for the earlier shallow activity and using manually refined relative relocations for events after 2 May, which includes all the deep activity. During the first three weeks of the summit eruption, until 3 May, CMM detected only sparse activity deeper than 10 km. In order to constrain the deep activity further, manual time picking was attempted for all 510 CMM-located events with SNR > 2.0 and with epicenters inside the region 63.58–63.70° latitude and 19.50–19.70° W longitude during 3–17 May. A total of 124 (24%) of these events were rejected as either false (where visual inspection showed that CMM had triggered on an incorrect signal) or, more frequently, where too few arrivals were sufficiently clear to make manual arrival time picks with high confidence. Events with an azimuthal gap

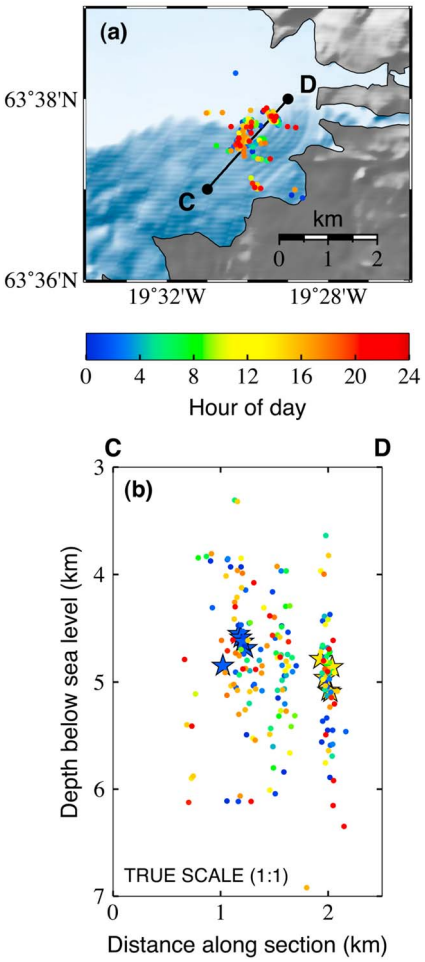

Figure 6. Refined locations obtained by using manual P- and S-wave arrival time picks and the HypoDD double-difference relative relocation algorithm [*Waldhauser and Ellsworth*, 2000] for 204 events on 14 March 2010. Hypocenters (dots) are color-coded by hour of the day. (a) Map view. (b) Cross-section along line C–D shown in Figure 6a, which is along the northeast-southwest axis of elongation evident in several clusters and approximately perpendicular to the cross-section in Figure 5b. Note the tight, sub-vertical lineation described by events at ~2 km along the cross-section, near D. Two other sub-vertical lineations are less clear at ~1.2 km and ~1.6 km along the cross-section from C: these can be seen more clearly in Animation 1. Stars show the locations of two sets of five events with closely similar waveforms. Mean relative location errors reported by HypoDD are ~80 m vertical and ~20 m horizontal.

greater than 180° between stations with manual phase picks were also rejected a priori, as were events with fewer than six clear phase picks. Most rejected events had CMM locations with SNR < 2.5, located less than 5 km b.s.l. under the summit eruption site.

[25] The relocated hypocenters lie in a series of clusters on a sub-linear trend, plunging steeply (80–85°) to the east, from the summit crater down to ~30 km depth, 4 km further east. The clusters have vertical gaps of up to ~3 km between them, where no events were observed during 3–17 May. The two largest clusters occurred at ~19 km and ~24 km depth respectively. Each of these clusters contains more than 100 relocated earthquakes, with the majority of events in both cases occurring over a period of a few hours on 10 May and 15 May respectively. The similarities between these two deep clusters in extent and geometry may indicate that they have similar trigger mechanisms.

[26] The time sequence of events during this period (shown by color-coding in Figure 7) indicates that activity occurred in bursts with different depth ranges active at different times. At a macroscopic level (rather than within individual clusters), it is notable that seismic activity tended to jump sporadically between different depths within the conduit, and there is a tendency for the largest clusters to occur at increasing depths with time.

5. Discussion

5.1. Complex Intrusion Prior to the Eruptions

[27] The pattern of seismicity suggests that pre-eruption intrusions under the northeastern flank of Eyjafjallajökull during March 2010 involved a series of sub-vertical pipes and dikes, some of which exhibit a NE-SW elongation as well as vertical elongation, forming a sub-parallel en echelon pattern radiating away from the summit of the volcano (Figure 5). The NE-SW elongation of the seismic clusters aligns with the strike of fissure swarms within the Eastern Volcanic Zone (Figure 1). The orientation of seismically inferred dikes is also consistent with dikes mapped at the surface by *Loughlin* [1995], who found that the majority of dike strike observations for 118 dikes mapped on the south side of Eyjafjallajökull lie in a bell-shaped distribution centered on ~N045°E.

[28] Seismic activity switched between separate clusters in discrete locations during the two weeks leading up to the first eruption at Fimmvörðuháls on 20 March 2010. We interpret all of the seismic activity in this period as being related to magma movement in these locations on different days.

[29] The finer structural detail obtained by manually refining arrival time picks and relocating events in one of these clusters reveals three sub-linear seismic clusters each with a vertical extent of 1–2 km (Figure 6 and Animation 1). We interpret these as delineating either three separate magma pipes, or the regions of brittle fracture at the edges of dikes with the same sub-vertical orientation.

[30] Determination of the shallowest vertical extent of these clusters may be limited by the geometry of the seismic network. Earthquake sources shallower than ~4 km under the northeastern flank of Eyjafjallajökull are not well resolved by the network configuration deployed during the eruptions because of a lack of sensors deployed directly overhead on the glacier [*Tarasewicz et al.*, 2011]. As such, the location process for the clusters shown in Figure 6 may have excluded earthquakes at shallower levels than the ~4 km upper limit of the clusters. The shallowest activity shown in Figures 2 and 5 is also relatively poorly constrained compared to the great majority of events recorded, which lie between 3.5 and 6.0 km depth b.s.l.

[31] Surface deformation, as measured by InSAR and GPS between 1 and 20 March, has been modeled by an inflating sill at a depth of 3.9–6.0 km in conjunction with a single inflating southeast-tilted dike extending from 3.2 to 6.1 km up to within a few hundred meters, or less, of the surface [*Sigmundsson et al.*, 2010]. These modeled depths are

relative to an average reference surface at ~400–500 m a.s.l. The seismicity we have recorded lies across the depth range of the modeled sill, and our earthquake locations could be consistent with dikes rising into a sill (and terminating) at ~4 km b.s.l., or with dikes rising up from a deeper sill at ~6 km b.s.l., or indeed a combination of both between sills at both ~4 km and ~6 km depth b.s.l.

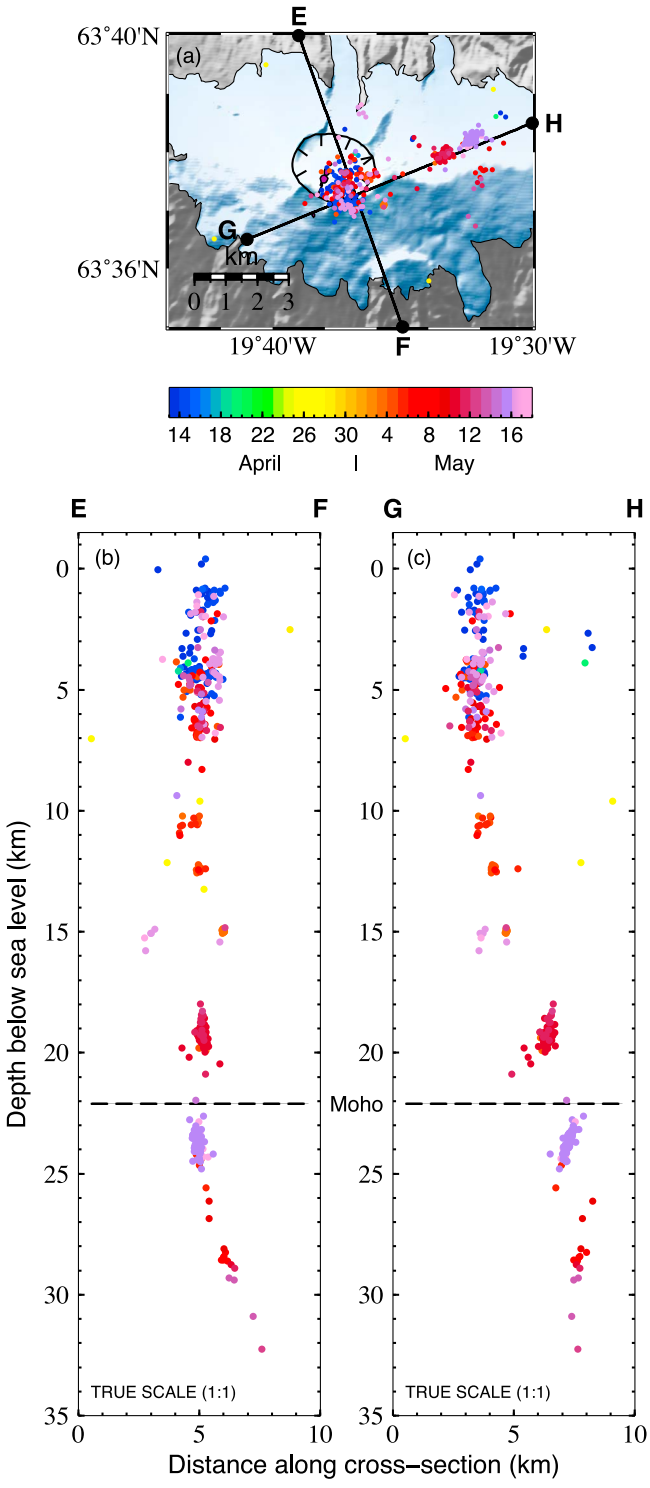

[32] The pattern of seismicity does not directly indicate lateral propagation or inflation of sills. If there were no sill, melt could be permeating a broad region in a series of vertical melt injections. However, it seems likely that buoyancy forces would encourage magma to pond into one or more sub-horizontal sills or magma chambers, rather than residing solely in the vertically elongated narrow dikes and pipes which are the main feature of the seismicity. An inflating sill may generate less seismicity than dikes because the local strain rates induced at the edges of a sill by the incremental addition of small volumes of melt to an existing, relatively voluminous, melt body will tend to be significantly lower than those induced by even small volumes of melt rising through unfractured country rock or narrow conduits. Hence it is likely that there are one or more sills that are responsible for much of the observed surface deformation, fed by (and/or drained by) the dikes that are imaged by the seismicity.

[33] Our favored interpretation is that batches of magma, which had accumulated beneath the eastern flank of the volcano during recent periods of unrest (1994 and 1999), were replenished with fresh intrusions from the mantle in late 2009 and early 2010. As with previous events, the magma accumulation was mostly confined to the northeast flank. During March 2010, sporadic injections of melt in a series of sub-vertical dikes and pipes occurred, possibly sourced from a sill which was inflating, largely aseismically, at ~6 km b.s.l., and some of those dikes may have terminated in a second sill at ~4 km b.s.l. Although the surface deformation indicates that the flank of the volcano was still inflating during the two weeks prior to the Fimmvörðuháls eruption on 20 March [*Sigmundsson et al.*, 2010], we have not found seismicity associated with a deep conduit during that period.

[34] The depth range of the seismicity under the northeast flank of the glacier lies within the expected horizon of neutral buoyancy in this setting [*Ryan*, 1987]. The relatively large lateral extent (~6 km east-west, ~3 km north-south) of the seismically active region, and the first-order temporal migration of seismicity laterally within the 3–6 km b.s.l. depth range toward Fimmvörðuháls prior to the eruption (Figure 5), are also consistent with the melt being neutrally buoyant at those depths. The sub-vertical seismic clusters observed in Figures 5 and 6 may reflect injections of melt that are initially driven by positive buoyancy, but then stagnate and fail to advance further as they become neutrally and negatively buoyant at shallower depths.

Figure 7. (a) Map view of hypocenter locations from 13 April to 17 May 2010, color-coded by date. 194 events are plotted from 13 April to 2 May 2010 which were obtained using CMM; those plotted have SNR > 2.4 and are all shallower than 10 km. The remaining 386 hypocenters plotted are from 3 to 17 May 2010 and are all manually refined, relative relocations obtained using HypoDD. (b and c) Cross-sections along approximately orthogonal lines E–F and G–H shown in Figure 7a, respectively, showing the depth distribution of the same hypocenters as in Figure 7a. Dashed line shows the estimated depth of the Moho [*Darbyshire et al.*, 2000; *Brandsdóttir and Menke*, 2008; *Vogfjörð et al.*, 2002]. See also Animation 2.

[35] We do not find any seismic evidence for the intrusive complex under the northeastern flank of Eyjafjallajökull, which fed the first eruption at Fimmvörðuháls, being linked to the geodetically inferred deflation source directly beneath the summit crater where the second eruption occurred.

5.2. Magma-Induced Earthquakes From the Mantle to the Surface

[36] During May 2010, starting three weeks after the onset of the Eyjafjallajökull summit eruption, we recorded a sequence of earthquakes over a two-week period that lie on a sub-linear trend from the summit eruption site down to ~30 km below sea level (Figure 7). Besides the coincident timing with the eruptive activity, the depth of these earthquakes provides some of the strongest evidence that they are caused by magma movement: many of these events occur well below the brittle-ductile transition in Iceland for tectonic strain rates [e.g., *Key et al.*, 2011a, 2011b] and therefore require a mechanism such as magma movement to generate locally high strain rates sufficient to cause brittle fracture.

[37] The character of the arrival waveforms (Figure 8), displaying clear impulsive P- and S-wave arrivals and relatively high frequency content (P wave arrivals typically peak at 8–12 Hz), indicates that these earthquakes are 'volcano-tectonic' events generated by brittle failure rather than other types of characteristic volcanic seismicity, such as tremor or other low-frequency signals.

[38] The crustal thickness in the Eyjafjallajökull region has been estimated as 22–23 km based on a combination of wide-angle reflection and refraction profiling and gravity modeling [*Darbyshire et al.*, 2000; *Brandsdóttir and Menke*, 2008; *Vogfjörð et al.*, 2002]. Even accounting for possible inaccuracies in our velocity model, we have recorded many events during the Eyjafjallajökull summit eruption at considerably greater depth than the base of the crust, including some in excess of 30 km. The most prominent clusters are at ~19 and ~24 km depth, consisting of 105 and 106 events respectively. These are close to the inferred crust-mantle boundary, so may be caused by a change in physical properties of the country rock in this transition region. Our results provide remarkably clear evidence of melt feeding into the lower crust from the mantle. The location of these deeper clusters lies to the east of the summit crater and directly beneath the shallow zone of intense seismicity at 3–6 km b.s.l. recorded prior to the Fimmvörðuháls fissure eruption (Figures 5 and 7). This may indicate a common deep upwelling source for both the flank and summit eruptions.

[39] Seismicity in the mid- and lower crust attributed to magma movement has been recorded elsewhere in Iceland [*Key et al.*, 2011a, 2011b; *White et al.*, 2011; *Martens et al.*, 2011], but observations of such earthquakes in the mantle are extremely rare. *Hjaltadóttir et al.* [2009] reported a swarm of earthquakes at 18–26 km depth beneath Eyjafjallajökull during 1996 with hypocenters directly beneath and also immediately north of the summit crater. These locations are 4–5 km west and west-northwest of the deepest seismicity we have observed, but are in the same depth range, as the two most prominent clusters we have located at ~19 km and ~24 km depth.

5.3. Possible Fracturing Mechanisms

[40] We have shown already that the earthquakes from both deep and shallow locations exhibit the characteristics of brittle fracturing, which generates clear P- and S-wave arrivals (Figure 8). What is also illustrated in Figure 8 is that we find some subsets of earthquakes within clusters with remarkably similar waveforms, often with several of these events occurring over a time period of a few minutes. These events are spatially close together, as is shown for the events in Figures 8a and 8b, which are plotted as stars in the depth profile shown in Figure 6. Besides being located close together, the similarity of waveforms and polarities also suggests that the fault planes and slip directions are similarly oriented within these subsets of events. These subsets of events that are ostensibly co-located to within the location uncertainty, with similar source mechanisms, therefore require a source process which is repeatable in a similar orientation many times in the space of a few minutes.

[41] We note that almost all of the activity in the deep sequence below ~12 km depth occurs in relatively tight spatial clusters with aseismic gaps of up to 3–4 km vertically between clusters (Figure 7). The largest clusters in this deep sequence occur at ~19 km and ~24 km depth and each individual cluster has a vertical extent of only ~1–2 km. Although most of the events in both of these clusters occurred over a period of just a few hours in each case, both locations also exhibit minor seismicity at other times during the two-week period of the deep sequence. If melt moved in the regions between clusters during the observation period, it appears to have done so aseismically and may represent regions where melt was able to flow along open conduits.

[42] The persistent activity in the same locations, in addition to the similar waveforms, suggests mechanisms that occur at restrictions or bottlenecks in a magma conduit, which may be causing seismicity in an otherwise aseismic conduit. One such mechanism could be a solidified magma plug being progressively shunted along a conduit by the pressure of magma beneath, such as has been suggested by *White et al.* [2011] to explain a sequence of almost identical events observed in the mid-crust at Upptyppingar in Iceland.

[43] Alternatively, it may be that the earthquake clusters and persistently active locations occur at bottlenecks or pinch-points that act as pressure-valves where magma is escaping periodically from an over-pressured sill at a

Figure 8. Examples of similar sets of waveforms, in each case displaying five arrivals from subsequent events all recorded at station ESK (see Figure 2 for location) and band pass filtered between 6 and 25 Hz. (a) Vertical component traces from the shallow dike in Figure 6 on 14 March (hypocenters are plotted as blue stars in Figure 6b). (b) Vertical component traces with a different characteristic waveform from a second sub-cluster at a similar depth to those shown in Figure 8a, also on 14 March (plotted as yellow stars in Figure 6b). (c) Vertical component traces from the cluster at ~19 km below sea level on 10 May. (d) Vertical component traces from the cluster at ~24 km below sea level on 15 May. (e and f) Horizontal (top) E–W and (bottom) N–S component traces for the same events shown in Figures 8c and 8d respectively. Note that all events have impulsive P wave arrivals and clear S-phases, indicating that even the deepest events exhibit characteristics of brittle failure likely to be associated with high strain rates caused by magma migration.

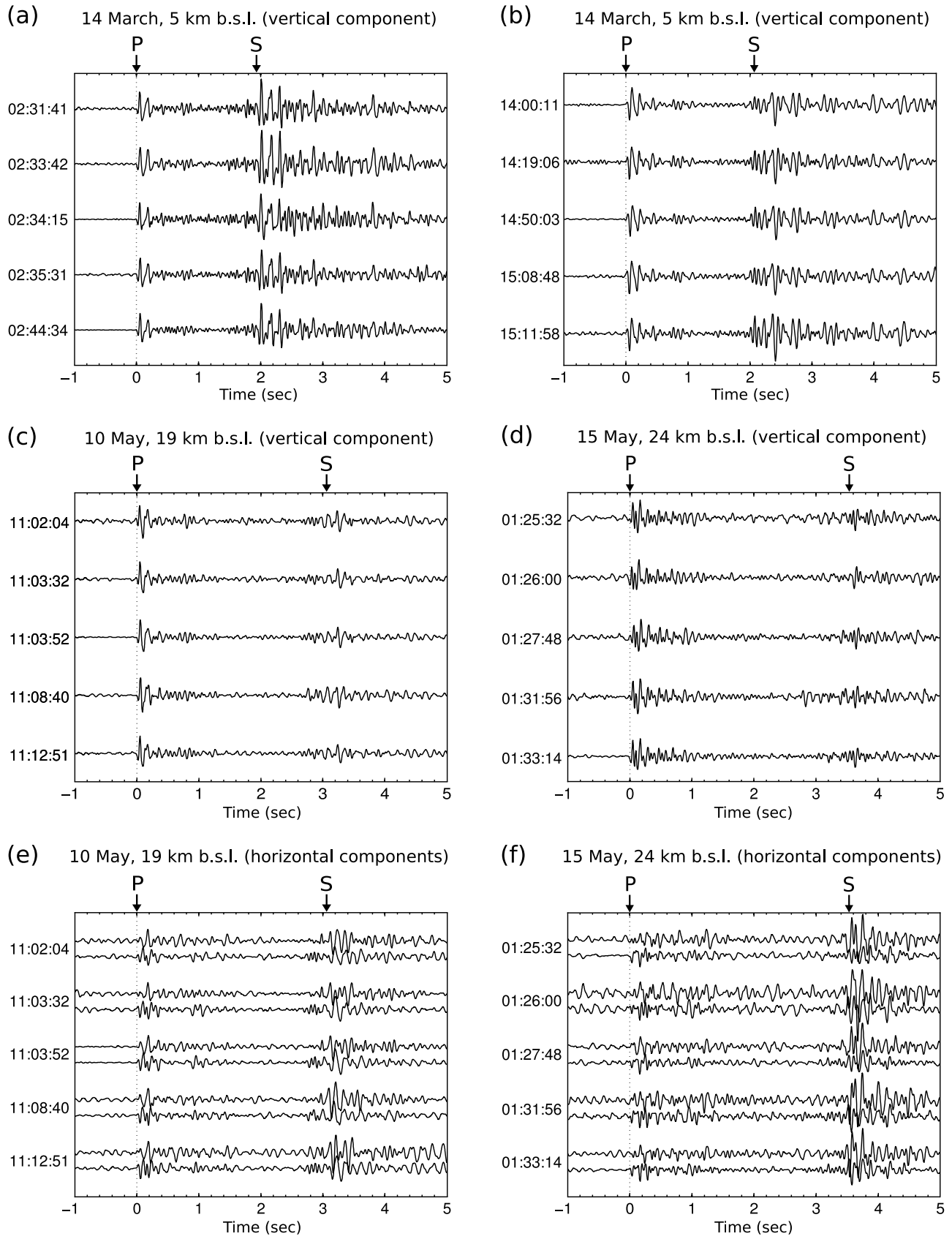
(a)
14 March, 5 km b.s.l. (vertical component)
P
S
02:31:41
02:33:42
02:34:15
02:35:31
02:44:34
−1 0 1 2 3 4 5
Time (sec)
(b)
14 March, 5 km b.s.l. (vertical component)
P
S
14:00:11
14:19:06
14:50:03
15:08:48
15:11:58
−1 0 1 2 3 4 5
Time (sec)
(c)
10 May, 19 km b.s.l. (vertical component)
P
S
11:02:04
11:03:32
11:03:52
11:08:40
11:12:51
−1 0 1 2 3 4 5
Time (sec)
(d)
15 May, 24 km b.s.l. (vertical component)
P
S
01:25:32
01:26:00
01:27:48
01:31:56
01:33:14
−1 0 1 2 3 4 5
Time (sec)
(e)
10 May, 19 km b.s.l. (horizontal components)
P
S
11:02:04
11:03:32
11:03:52
11:08:40
11:12:51
−1 0 1 2 3 4 5
Time (sec)
(f)
15 May, 24 km b.s.l. (horizontal components)
P
S
01:25:32
01:26:00
01:27:48
01:31:56
01:33:14
−1 0 1 2 3 4 5
Time (sec)

Figure 8

rheological boundary of some sort, and could hint at the position of magma storage locations at depth. Petrological arguments suggest that melt does pond at different depths in the upper mantle and crust beneath Iceland [*Maclennan et al.*, 2001] and sills emplaced into mantle rocks have been exhumed in exposed ophiolites in Oman [e.g., *Boudier and Nicolas*, 1995; *Kelemen et al.*, 1997].

[44] Another mechanism that could produce similar waveforms might be the propagation of a dike tip over a short distance, perhaps re-fracturing a previously open conduit which has solidified; numerical and physical modeling indicates that the orientation of dike propagation may be constant over large distances, provided that the physical properties of the rock through which it is propagating are constant [*Maccaferri et al.*, 2010]. A series of small propagation steps might produce seismically similar events and appear to be co-located to within our location resolution. However, it is unlikely that this is the case for the larger sequences of 15–20 earthquakes with similar waveforms, because the tip would then advance far enough for the migration to be resolved from the locations of the micro-earthquakes and for the waveforms to change. It is likely that this sort of fracturing or re-fracturing mechanism is responsible for some of the earthquakes observed, but without generating obviously similar waveforms. Alternatively, some earthquakes may be occurring in the country rock in the zones of maximum shear stress that lie at 45° to the dike orientation at a dike tip or bottleneck in a conduit [e.g., *Hill*, 1977].

[45] Many of the seismic events observed do not occur in groups with obviously similar waveforms. These could have a variety of source processes either in solidified magma in a previously open conduit, or fracturing of the surrounding country rock. For instance, hot magma may locally weaken the rock around the conduit; if there is sufficiently high ambient differential stress, this may result in stress transfer onto the adjacent rock volume that causes brittle failure. At the shallowest levels, magma may also have interacted with groundwater and caused geothermal seismic activity.

[46] Focal mechanism solutions could be used to constrain which of these fracturing mechanisms is responsible for a particular event, or cluster. We should expect to see both normal and reverse faulting along similar fault planes aligned with the conduit for events caused by shunting or fracturing of a plug, as described by *White et al.* [2011]. By contrast, cracking in the zones of maximum shear stress around dike tips should be on failure planes that are inclined at 30–60° to the dike. Earthquake source mechanisms with a greater isotropic, explosive component might be expected for fracturing at bottlenecks in a conduit, or cracking open the extending tip of a dike. *Hensch et al.* [2010] found evidence for both reverse and normal faulting source mechanisms in the shallow seismicity, but further work is required to be able confidently to distinguish between the various mechanisms outlined above.

5.4. Interpretation of the Timing of Activity Across the Depth Range

[47] While there are instances of directional migration in some individual clusters, we do not observe any consistent progression of activity at a macroscopic level from depth to the surface, or vice versa, in the deep sequence of events in May 2010 shown in Figure 7. Instead, there is continual activity at depths shallower than ~12 km, which is ongoing for most of the period, accompanied by more sporadic activity between 12 and 30 km depth; the location of seismic activity jumps regularly. To first order, it is notable that the shallower of the two major deep swarms, at ~19 km depth, precedes the later swarm at ~24 km depth, with activity between ~10–15 km preceding both. In fact, very little seismicity deeper than ~12 km is observed until three weeks after the summit eruption started. Similarly, on a smaller scale, the sequence of events recorded on 14 March in the shallow dikes shown in Figure 6 shows contemporaneous fracturing along the ~2 km height of the dike rather than a progression from bottom to top.

[48] These observations on the timing of activity suggest that we have not recorded seismicity generated by a pulse of melt rising all the way from the mantle to the surface, or even from the bottom to the top of a much smaller dike. Rather, we have observed mechanisms within pre-existing conduits, which sporadically produce seismicity by the mechanisms discussed above.

[49] We speculate that the time lag of three weeks after onset of the explosive summit eruption before any deep seismicity is observed could be the result of two contributing factors. First, the pressure release at the top of the system by eruption of volcanic material and unloading of ice as it melted and flowed away could have fed back through the system and mobilized progressively deeper pockets of melt. The magma plumbing system at shallow levels must have been at critical pressure immediately before the summit eruption started, and the removal of mass from shallow levels would reduce the pressure in shallow magma chambers. If these are linked by open conduits to greater depth, then we might expect to see a response at depth simply as a result of this surface unloading.

[50] Assuming that a thickness of approximately 200 m of ice [*Gudmundsson et al.*, 2010a] with a density of 0.92×10^3 kg/m^3 was melted and then drained away as glacial floodwater, that would result in a pressure reduction of approximately 1.8 MPa over the area of the ice cauldrons in the summit crater simply from unloading the ice mass. Furthermore, approximately 0.1 km^3 of magma is estimated to have been erupted from the summit crater by early May [*Gudmundsson et al.*, 2010b], much of which was removed from the immediate area as airborne ash. If we make the assumption that this magma came from a deflating magma chamber vertically beneath the surface summit crater which was of the same ~2 km diameter, then that would produce further unloading beneath the magma chamber equivalent to approximately 0.9 MPa, or a total pressure reduction of ~2.5–3.0 MPa. Separately to the effect of removing part of the overburden, the removal of material from inside the magma chamber would also reduce the magmatic overpressure in the chamber. This pressure reduction by unloading of ice and magma must have a feedback effect to some extent on the shallow magma chamber and perhaps also on the deeper plumbing system. The reduction in overburden pressure alone is of the same order of magnitude as the stress drops commonly observed for small earthquakes [*Shearer et al.*, 2006].

[51] Second, we propose that a change in flow conditions in the conduit could cause a previously aseismic conduit to

become seismogenic. This might be achieved as a result of a reduction in flow rate in an active conduit such that bottlenecks start to clog up as slow-moving melt starts to solidify; these plugs of frozen magma would therefore need to be re-fractured to allow any subsequent flow of melt through the conduit. Conversely, a sharp increase in melt supply could force the conduit to open further, albeit this would seem more likely to produce a sequence of clusters where melt pockets become over-pressured at progressively shallower depths. Clearly magma movement at these depths is often aseismic, or at least is very rarely observed. For instance, the surface deformation during emplacement of the shallow flank intrusions in March requires substantial magma influx at estimated rates of 30–40 m^3s^{-1} [*Sigmundsson et al.*, 2010], yet we do not observe any convincing deep seismicity associated with it. While we recognize that it is possible that we have overlooked some deep earthquakes during this period due to the intense shallow seismic activity, it is also possible that there were one or more active conduits that were continuously open during this period with magma flow from the mid and lower crust feeding the shallow intrusions without producing seismicity. Figure 7 shows that the locations of the deepest clusters we observe during the summit eruption are directly beneath the early shallow intrusion complex under the northeastern flank of the glacier, so it may be the case that the same deep source region fed both that intrusion and a magma chamber directly beneath the summit crater of the second eruption, even without any clear connection between the two at shallow levels.

6. Conclusions

[52] 1. We have used an automatic Coalescence Microseismic Mapping (CMM) technique to detect and locate several thousand earthquakes associated with magma movement in a series of sub-vertical dikes, striking northeast-southwest, in an intrusion complex under the northeastern flank of the Eyjafjallajökull glacier during the two weeks prior to the Fimmvörðuháls flank eruption.

[53] 2. During the second, explosive, Eyjafjallajökull summit eruption we have located magma-induced earthquakes along a sub-linear trend extending sub-vertically from ~30 km depth to the surface. This is a rare observation of melt feeding into the lower crust from the mantle, which is usually either aseismic or is not monitored with a sufficiently dense network to be observed.

[54] 3. Spatial clustering of earthquakes, particularly in the depth range 12–30 km with aseismic gaps between them, suggests that seismic activity is concentrated at restrictions or bottlenecks in an otherwise aseismic magma conduit. The position of these clusters may hint at positions of rheological boundaries and possibly locations of magma storage if they are related to exit points from over-pressured melt pockets. The two largest clusters of seismic activity at ~19 km and ~24 km depth straddle the inferred depth of the Moho, which is a major rheological and compositional boundary between crust and mantle.

[55] 4. Subsets of earthquakes within the main spatial clusters have similar waveforms and are temporally clustered, often occurring within minutes of one another. This observation requires that the source process for these subsets of events is repeatable multiple times, in approximately the same place, with a similarly oriented source mechanism. This might be achieved by repeated pulses of melt escaping from a melt body as it is fed from below, or alternatively could be generated by a solidified magma plug being forced along a conduit.

[56] 5. The seismic activity in the two-week long sequence of deep events observed in May 2010 does not show a clear progression in depth, but jumps between deep and shallow levels during the Eyjafjallajökull summit eruption. The bulk of the deep (>12 km) seismic activity does not occur until approximately three weeks after the summit eruption starts, after which the largest clusters show a deepening progression down to at least 25 km depth. The time delay and subsequent deepening of significant swarms may reflect the response to a pressure reduction at shallow levels arising from the removal of ice and magma, which feeds back down the plumbing system mobilizing melt pockets at progressively greater depths. It may also reflect a change in flow conditions in the conduit, causing a transition from aseismic to seismogenic magma migration, for instance as a result of a drop in flow rate.

[57] **Acknowledgments.** The temporary stations used in this study are from the LOKI instrument pool, which is jointly owned by the Icelandic Meteorological Office, the Institute of Earth Sciences, University of Iceland and the Iceland GeoSurvey. We thank Sveinbjörn Steinþórsson, Þorsteinn Jónsson, Ólafur Guðmundsson, Benedikt Ófeigsson and numerous other scientists and graduate students who assisted with the fieldwork. We also thank the landowners at Seljavellir, Núpar and Barkarstaðir for housing the seismic stations sel, nup and bark. The Icelandic Coast Guard helicopter was used to retrieve the gij station following the floods from Gígjökull on 14 April 2010. Julian Drew provided and helped with the CMM software, and Hilary Martens wrote Matlab code used for picking arrival times. Finnur Pálsson, Eyjólfur Magnússon and Ásta Rut Hjartardóttir provided recent digitized data of glacier outlines, eruption sites and tectonic features. Generic Mapping Tools [*Wessel and Smith*, 1998] were used to produce the figures. We thank Michael Ryan, Allan Rubin, Fred Klein and an anonymous reviewer for their helpful comments. JT is funded by a NERC studentship and CASE award supported by ERC Equipoise Ltd. Dept. Earth Sciences, Cambridge, contribution ESC2248.

References

Bjarnason, I. T., W. Menke, O. G. Flóvenz, and D. Caress (1993), Tomographic image of the mid-Atlantic plate boundary in southwestern Iceland, *J. Geophys. Res.*, *98*, 6607–6622, doi:10.1029/92JB02412.

Boudier, F., and A. Nicolas (1995), Nature of the Moho transition zone in the Oman ophiolite, *J. Petrol.*, *36*(3), 777–796.

Brandsdóttir, B., and W. H. Menke (2008), The seismic structure of Iceland, *Jökull*, *58*, 17–34.

Brandsdóttir, B., M. Parsons, R. S. White, O. Guðmundsson, J. Drew, and B. S. Thorbjarnardóttir (2010), The May 29th 2008 earthquake aftershock sequence within the South Iceland Seismic Zone: Fault locations and source parameters of aftershocks, *Jökull*, *60*, 1–22.

Dahm, T., and B. Brandsdóttir (1997), Moment tensors of microearthquakes from the Eyjafjallajökull volcano in south Iceland, *Geophys. J. Int.*, *130*, 183–192, doi:10.1111/j.1365-246X.1997.tb00997.x.

Darbyshire, F., R. White, and K. Priestley (2000), Structure of the crust and uppermost mantle of Iceland from a combined seismic and gravity study, *Earth Planet. Sci. Lett.*, *181*, 409–428, doi:10.1016/S0012-821X(00)00206-5.

Drew, J. (2010), Coalescence microseismic mapping: An imaging method for the detection and location of seismic events, PhD dissertation, Univ. of Cambridge, Cambridge, U. K.

Einarsson, P. (1991), Earthquakes and present-day tectonism in Iceland, *Tectonophysics*, *189*, 261–279, doi:10.1016/0040-1951(91)90501-I.

Einarsson, P., and B. Brandsdóttir (2000), Earthquakes in the Mýrdalsjökull area, Iceland, 1978–1985: Seasonal correlation and connection with volcanoes, *Jökull*, *49*, 59–73.

Einarsson, P., and K. Sæmundsson (1987), Earthquake epicenters 1982–1985 and volcanic systems in Iceland, in *Í Hlutarins Eðli: Festschrift for Thorbjorn Sigurgeirsson*, edited by T. Sigfússon, Menningarsjóður, Reykjavík.

Gudmundsson, M. T., et al. (2010a), The Eyjafjallajökull eruption in April-May 2010: Course of events, ash generation and ash dispersal, Abstract

V53F-01 presented at 2010 Fall Meeting, AGU, San Francisco, Calif., 13–17 Dec.

Gudmundsson, M. T., R. Pedersen, K. Vogfjörd, B. Thorbjarnardóttir, S. Jakobsdóttir, and M. J. Roberts (2010b), Eruptions of Eyjafjallajökull Volcano, Iceland, *Eos Trans. AGU*, *91*(21), 190, doi:10.1029/2010EO210002.

Gudmundsson, O., B. Brandsdóttir, W. Menke, and G. E. Sigvaldason (1994), The crustal magma chamber of the Katla volcano in south Iceland revealed by 2-D seismic undershooting, *Geophys. J. Int.*, *119*, 277–296, doi:10.1111/j.1365-246X.1994.tb00928.x.

Hensch, M., B. Brandsdóttir, T. Árnadóttir, A. Auriac, and B. S. Thorbjarnardóttir (2010), Intrusive activity beneath Eyjafjallajökull 1991–2010 from analysis of earthquake and geodetic data, Abstract V21F-05 presented at 2010 Fall Meeting, AGU, San Francisco, Calif., 13–17 Dec.

Hill, D. P. (1977), A model for earthquake swarms, *J. Geophys. Res.*, *82*, 1347–1352.

Hjaltadóttir, S., K. S. Vogfjörð, and R. Slunga (2009), Seismic signs of magma pathways through the crust in the Eyjafjallajökull volcano, south Iceland, *Rep. VI 2009-13*, Icelandic Meteorol. Off., Reykjavik.

Jakobsdóttir, S. S. (2008), Seismicity in Iceland: 1994–2007, *Jökull*, *58*, 75–100.

Jóhannesson, H., and K. Sæmundsson (1998), Geological map of Iceland, bedrock geology, scale 1:500,000, Icelandic Inst. of Natl. Hist. and Icelandic Geod. Surv., Reykjavík.

Kelemen, P., K. Koga, and N. Shimizu (1997), Geochemistry of gabbro sills in the crust-mantle transition zone of the Oman ophiolite: Implications for the origin of the oceanic lower crust, *Earth Planet. Sci. Lett.*, *146*, 475–488, doi:10.1016/S0012-821X(96)00235-X.

Key, J., R. S. White, H. E. Soosalu, and S. S. Jakobsdóttir (2011a), Multiple melt injection along a spreading segment at Askja, Iceland, *Geophys. Res. Lett.*, *38*, L05301, doi:10.1029/2010GL046264.

Key, J., R. S. White, H. Soosalu, and S. S. Jakobsdóttir (2011b), Correction to "Multiple melt injection along a spreading segment at Askja, Iceland," *Geophys. Res. Lett.*, *38*, L10308, doi:10.1029/2011GL047491.

Klein, F. W. (2002), User's guide to HYPOINVERSE-2000, a FORTRAN program to solve for earthquake locations and magnitudes, *U.S. Geol. Surv. Open File Rep.*, *02-171*, 123 pp.

Larsen, G. (1999), Gosið í Eyjafjallajökli 1821–23, *Rep. RH-28-99*, 13 pp., Sci. Inst., Univ. of Iceland, Reykjavík.

Larsen, G. (2000), Holocene eruptions within the Katla volcanic system, south Iceland: Characteristics and environmental impact, *Jökull*, *49*, 1–28.

Loughlin, S. C. (1995), The evolution of the Eyjafjöll volcanic system, southern Iceland, PhD thesis, Univ. of Durham, Durham, U. K.

Maccaferri, F., M. Bonafede, and E. Rivalta (2010), A numerical model of dyke propagation in layered elastic media, *Geophys. J. Int.*, *180*, 1107–1123, doi:10.1111/j.1365-246X.2009.04495.x.

Maclennan, J., D. McKenzie, K. Gronvold, and L. Slater (2001), Crustal accretion under northern Iceland, *Earth Planet. Sci. Lett.*, *191*, 295–310, doi:10.1016/S0012-821X(01)00420-4.

Martens, H. R., R. S. White, J. Key, J. Drew, H. Soosalu, and S. S. Jakobsdóttir (2011), Dense seismic network provides new insight into the 2007 Upptyppingar dyke instrusion, *Jökull*, *60*, 47–66.

Óskarsson, B. V. (2009), The Skerin ridge on Eyjafjallajökull, south Iceland: Morphology and magma-ice interaction in an ice-confined silicic fissure eruption, MS thesis, Fac. of Earth Sci., Univ. of Iceland, Reykjavík.

Pedersen, R., and F. Sigmundsson (2004), InSAR based sill model links spatially offset areas of deformation and seismicity for the 1994 unrest episode at Eyjafjallajökull volcano, Iceland, *Geophys. Res. Lett.*, *31*, L14610, doi:10.1029/2004GL020368.

Pedersen, R., and F. Sigmundsson (2006), Temporal development of the 1999 intrusive episode in the Eyjafjallajökull volcano, Iceland, derived from InSAR images, *Bull. Volcanol.*, *68*, 377–393, doi:10.1007/s00445-005-0020-y.

Ryan, M. P. (1987), Neutral buoyancy and the mechanical evolution of magmatic systems, in *Magmatic Processes: Physicochemical Principles*, *Spec. Publ. Geochem. Soc.*, *1*, 259–288.

Shearer, P. M., G. A. Prieto, and E. Hauksson (2006), Comprehensive analysis of earthquake source spectra in Southern California, *J. Geophys. Res.*, *111*, B06303, doi:10.1029/2005JB003979.

Sigmundsson, F., et al. (2010), Intrusion triggering of the 2010 Eyjafjallajökull explosive eruption, *Nature*, *468*, 426–430, doi:10.1038/nature09558.

Sturkell, E., F. Sigmundsson, and P. Einarsson (2003), Recent unrest and magma movements at Eyjafjallajökull and Katla volcanoes, Iceland, *J. Geophys. Res.*, *108*(B8), 2369, doi:10.1029/2001JB000917.

Tarantola, A., and B. Valette (1982), Inverse problems–Quest for information, *J. Geophys.*, *50*, 159–170.

Tarasewicz, J., R. S. White, B. Brandsdóttir, and B. Thorbjarnardóttir (2011), Location accuracy of earthquake hypocentres beneath Eyjafjallajökull, Iceland, prior to the 2010 eruptions, *Jökull*, *61*, 33–50.

Thoroddsen, T. (1925), *Die Geschichte der Isländischen Vulkane*, 458 pp., A. F. Høst, Copenhagen.

Vogfjörð, K. S., et al. (2002), Crustal profiling in Iceland using earthquakes source arrays, *Eos Trans. AGU*, *83*(47), Fall Meet. Suppl., Abstract S61C-1161.

Wadati, K. (1933), On the travel time of earthquake waves, Part II, *Geophys. Mag.*, *7*, 101–111.

Waldhauser, F., and W. L. Ellsworth (2000), A double-difference earthquake location algorithm: Method and application to the Northern Hayward Fault, California, *Bull. Seismol. Soc. Am.*, *90*, 1353–1368, doi:10.1785/0120000006.

Wessel, P., and W. H. F. Smith (1998), New, improved version of the Generic Mapping Tools released, *Eos Trans. AGU*, *79*(47), 579, doi:10.1029/98EO00426.

White, R. S., J. Drew, H. K. Martens, A. J. Key, H. Soosalu, and S. S. Jakobsdóttir (2011), Dynamics of dyke intrusion in the mid-crust of Iceland, *Earth Planet. Sci. Lett.*, *304*, 300–312, doi:10.1016/j.epsl.2011.02.038.

B. Brandsdóttir and M. Hensch, Institute of Earth Sciences, Science Institute, University of Iceland, Askja, Sturlugata 7, 101 Reykjavík, Iceland.

J. Tarasewicz and R. S. White, Bullard Laboratories, University of Cambridge, Madingley Road, Cambridge CB3 0EZ, UK. (jptt2@cam.ac.uk)

B. Thorbjarnardóttir, Icelandic Meteorological Office, Bústaðavegur 9, 150 Reykjavík, Iceland.